

Thermo-Electro-Responsive Redox-Copolymers for Amplified Solvation, Morphological Control, and Tunable Ion Interactions

Raylin Chen, Hanyu Wang, Mathieu Doucet, James F. Browning, and Xiao Su*



Cite This: *JACS Au* 2023, 3, 3333–3344



Read Online

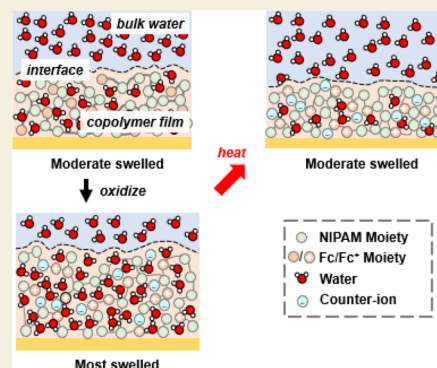
ACCESS |

Metrics & More

Article Recommendations

Supporting Information

ABSTRACT: Electro-responsive metallopolymers can possess highly specific and tunable ion interactions, and have been explored extensively as electrode materials for ion-selective separations. However, there remains a limited understanding of the role of solvation and polymer–solvent interactions in ion binding and selectivity. The elucidation of ion–solvent–polymer interactions, in combination with the rational design of tailored copolymers, can lead to new pathways for modulating ion selectivity and morphology. Here, we present thermo-electrochemical-responsive copolymer electrodes of *N*-isopropylacrylamide (NIPAM) and ferrocenylpropyl methacrylamide (FPMAm) with tunable polymer–solvent interactions through copolymer ratio, temperature, and electrochemical potential. As compared to the homopolymer PFPMAm, the P(NIPAM_{0.9}-co-FPMAm_{0.1}) copolymer ingressed 2 orders of magnitude more water molecules per doping ion when electrochemically oxidized, as measured by electrochemical quartz crystal microbalance. P(NIPAM_{0.9}-co-FPMAm_{0.1}) exhibited a unique thermo-electrochemically reversible response and swelled up to 83% after electrochemical oxidation, then deswelled below its original size upon raising the temperature from 20 to 40 °C, as measured through spectroscopic ellipsometry. Reduced P(NIPAM_{0.9}-co-FPMAm_{0.1}) had an inhomogeneous depth profile, with layers of low solvation. In contrast, oxidized P(NIPAM_{0.9}-co-FPMAm_{0.1}) displayed a more uniform and highly solvated depth profile, as measured through neutron reflectometry. P(NIPAM_{0.9}-co-FPMAm_{0.1}) and PFPMAm showed almost a fivefold difference in selectivity for target ions, evidence that polymer hydrophilicity plays a key role in determining ion partitioning between solvent and the polymer interface. Our work points to new macromolecular engineering strategies for tuning ion selectivity in stimuli-responsive materials.



KEYWORDS: *stimuli-responsive polymers, redox-electrochemistry, solvation, electrochemical separations*

1. INTRODUCTION

Stimuli-responsive materials have a wide range of applications, including sensors, actuators, electrochromic devices, and for separations.^{1–4} In particular, redox metallopolymers have gained attention as a platform for electrochemically switched capture and release of ions, with high capacity, selectivity, and molecular modularity.⁵ While there has been significant progress in elucidating the charge-transfer origins of selective binding and developing molecular design rules to tune selectivity, especially for ferrocene-based polymers,^{6,7} a deep understanding about the role of solvation in ion binding and whether solvation can be controlled through polymer–solvent affinity (hydrophobicity/hydrophilicity) remains elusive.⁸ Solvation underpins many phenomena of solutes in water, including protein folding,⁹ hydrophobic interactions,¹⁰ and specific ion effects, such as the Hofmeister series.¹¹ Surface engineering to tune hydrophobicity/hydrophilicity has been used to tune adhesion forces between surfaces,¹² control catalyst selectivity,¹³ and separate hydrophobic contaminants from water.¹⁴ For ion sorption, switching between surface hydrophobicity or hydrophilicity can change ion adsorption affinities to that surface and can even result in the reversal of

ion affinity trends.^{15,16} Despite growing understanding of the role of electrostatics and adsorbent-ion interactions, the relative strength of the solvation effects to charge-transfer effects is unknown.^{17,18} In addition, polymer adsorbents, especially in gel form, present not only a direct interface with water but also a deeper microenvironment with unique solvation properties—and in the case of responsive polymers, this microenvironment can be dramatically tuned by external stimuli. To advance the understanding and exert tailored control of polymer solvation on ion selectivity, we developed a copolymer system containing *N*-isopropylacrylamide (NIPAM) and ferrocene (Fc) moieties with temperature- and composition-dependent hydration (i.e., solvation for aqueous systems), to investigate ion selectivity under controlled solvation conditions.

Received: August 19, 2023

Revised: September 23, 2023

Accepted: September 29, 2023

Published: November 21, 2023



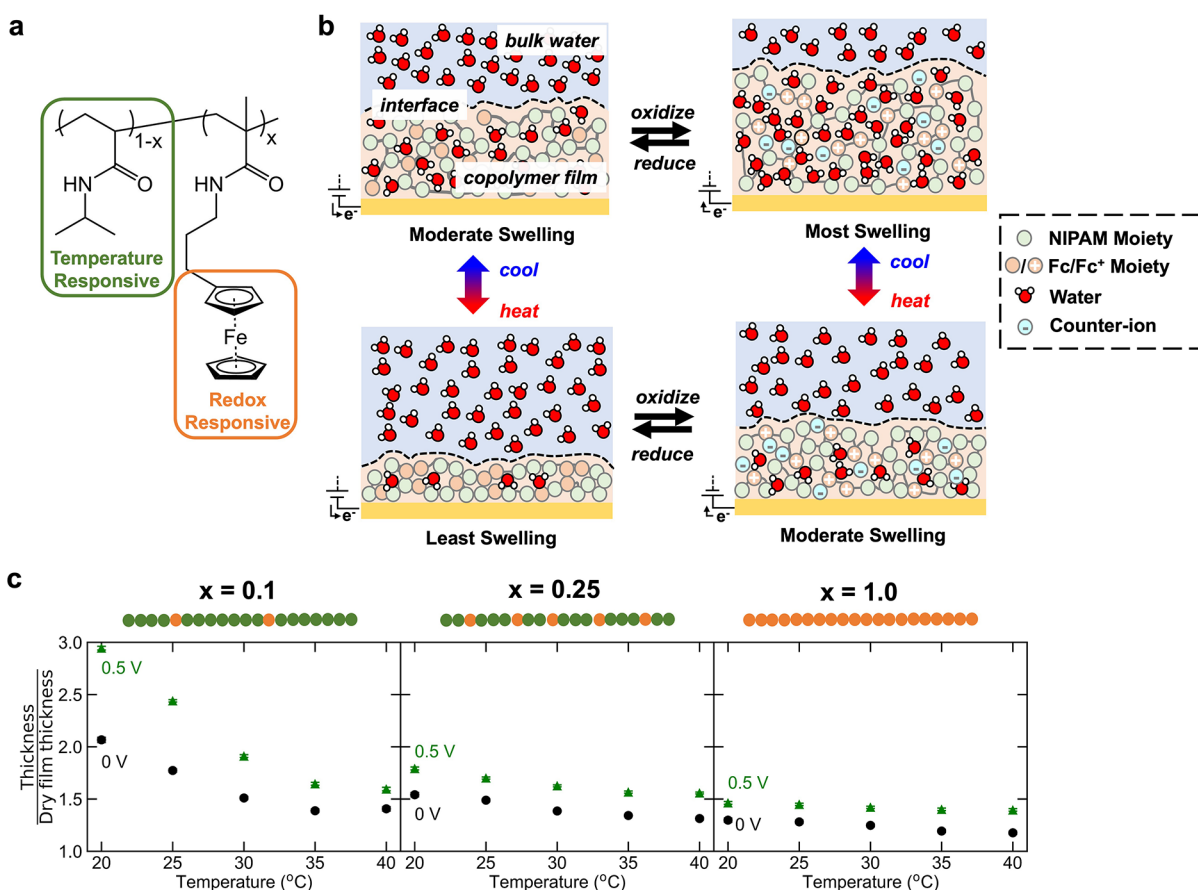


Figure 1. (a) P(NIPAM_{1-x}-co-FPMAM_x) representation. Highlighted in green: Thermoresponsive NIPAM moiety. Highlighted in orange: Redox/electrochemically responsive ferrocene moiety. (b) Schematic of the orthogonal dual temperature and electrochemically responsive P(NIPAM_{1-x}-co-FPMAM_x) swelling and deswelling. (c) P(NIPAM_{1-x}-co-FPMAM_x) thickness in 20 mM NaClO₄ solution, normalized by the polymer film thickness when dry, at an oxidizing potential (green) and reducing potential (black) at various temperature. FPMAM fraction (x) increases from 0.1, 0.25, to 1.0 left to right. Thickness was measured using in situ spectroscopic ellipsometry. Error bars represent 90% confidence limits on ellipsometry fitting.

Poly(*N*-isopropylacrylamide) (PNIPAM) is a thermoresponsive polymer that undergoes a solvation-governed phase transition at a lower critical solution temperature (LCST) of approximately 32 °C in water.¹⁹ Below the LCST, the moieties of PNIPAM are surrounded by hydration shells of water and, as a result, PNIPAM is soluble in water and PNIPAM gels are swelled with water.^{20,21} As the temperature increases, water loses its ability to surround the hydrophobic moieties, and the hydrophobic moieties are forced to aggregate or phase separate.²¹ For PNIPAM, this results in the LCST phase transition as PNIPAM chains dehydrate and collapse together. PNIPAM polymers or gels can leverage this hydrophilic-to-hydrophobic collapse for applications, such as drug delivery, smart actuators, and water treatment.^{22–24} In parallel, ferrocene (Fc) is a redox moiety with broad uses spanning catalysis, materials science, and medicinal chemistry.^{25,26} Ferrocene polymers have been used as charged and dielectric interfaces, redox gels, and in block copolymers for phase-separated materials.^{27,28} The redox transformation from neutral ferrocene to positive ferrocenium has enabled smart surfaces with switchable hydrophobicity/hydrophilicity and redox gels with switchable solvent swelling and solvent selectivity.^{29,30} In particular, ferrocene polymers have served as a platform for electrochemical separations, where the redox-switching between charged and neutral states enables the

electrochemical adsorption and release of charged species, and the modification of polymer structure allows for highly tunable interactions.^{18,31–33}

The combination of NIPAM and Fc moieties creates dual redox and thermoresponsive copolymers, with redox and thermoresponsive hydration.³⁴ Previous reports of NIPAM-Fc copolymers showed composition and redox-dependent LCSTs.^{35,36} NIPAM-VFc gels exhibited redox-potential dependent transition temperatures^{37,38} and showcased for a variety of applications.^{39–44} Interestingly, pathways for electrochemically and thermally induced phase transition have also been reported with nanocrystal systems.⁴ However, oxidation for the copolymer systems has been typically performed chemically rather than electrochemically, with a few studies correlating electrochemical activity by cyclic voltammogram (CV).⁴⁰ More recently, NIPAM-VFc microgels used for cargo shuttling were demonstrated to have electrochemical switchable swelling.⁴⁵ While these prior studies have provided fundamental insights, the electrochemical swelling and solvation properties for an immobilized NIPAM-Fc film are yet to be fully quantified and understood, especially within the framework of developing NIPAM-Fc copolymers as a platform for tunable hydration and stimuli-driven ion-selective separations.

In this work, we copolymerized NIPAM with ferrocenyl-propyl methacrylamide (FPMAM), a ferrocene-containing comonomer, for a P(NIPAM-*co*-FPMAM) system with temperature, redox, and copolymer composition dependent hydration as a platform for solvation-controlled ion separations. We report the first quantification of volume changes for an immobilized NIPAM-Fc gel film as a function of temperature and electrochemical input using in situ electrochemical spectroscopic ellipsometry. The quantification of film volume (i.e., thickness) serves as a proxy for quantifying film hydration. In situ measurements of electrochemical thin films using techniques, such as ellipsometry and neutron reflectometry (NR), have shed much light on redox polymer hydration and morphological dynamics during redox processes.^{46,47} Additionally, we report the first demonstration that the volume change from electrochemical response is reversible with a change in temperature and the first quantification of water ingress (hydration) into a NIPAM-Fc gel during electrochemical oxidation as a function of temperature using EQCM with analysis of multiple overtones. Through NR, we gain nanoscale insight into the spatial morphology of P(NIPAM-*co*-FPMAM) as a function of electrochemical potential. Finally, we evaluated the selectivity of copolymer electrodes at different NIPAM and FPMAM compositions to investigate how the hydration of the local microenvironment can play a role in ion selectivity. We envision our findings to provide new macromolecular engineering strategies for tuning ion selectivity in stimuli-responsive materials, expanding beyond the previous focus on single redox sites at a monomer level.

2. RESULTS AND DISCUSSION

2.1. Investigation of Thermo-Electrochemical-Responsive Morphology

First, we evaluate the morphological response of our tailored copolymers to thermal and electrochemical modulation using in situ ellipsometry techniques. P(NIPAM_{1-*x*}-*co*-FPMAM_{*x*}) with three FPMAM fractions (*x* = 0.1, 0.25, 1) were synthesized through a free radical polymerization method (Supporting Information S1), with the copolymer structure shown in Figure 1. P(NIPAM_{1-*x*}-*co*-FPMAM_{*x*}) copolymer films were spin coated on gold substrates and cross-linked via a thermally activated cross-linker benzene-1,3-disulfonyl azide, which cross-links through a C–H insertion mechanism.⁴⁸ The morphology of the copolymer films was examined with in situ electrochemical spectroscopic ellipsometry in 20 mM NaClO₄ from 20 to 40 °C, at reducing and oxidizing electrochemical potentials. Prior to the reported measurements, cross-linked P(NIPAM_{1-*x*}-*co*-FPMAM_{*x*}) films were fully swelled via cyclic voltammetry, until the peak current in the CVs no longer increased with subsequent cycles. This preemptive cycling ensured the largest volume-to-electrochemical response was exhibited and that subsequent measurements reflect the equilibrium temperature and potential conditions, rather than the transient behavior of initial swelling. Film thickness measurements during in situ electrochemical ellipsometry began at 20 °C at the reducing potential of the ferrocene units (0 V vs Ag/AgCl). The potential was scanned to an oxidizing potential (0.5 V vs Ag/AgCl), then lowered back to the reducing potential before the temperature was increased to 25 °C (Figure 1b). This procedure was repeated up to 40 °C in 5 °C increments. Copolymer film thickness was normalized

to the dry film thickness to account for individual sample variation.

The addition of NIPAM to PFPAM magnified both the electrochemical and temperature morphological response. Cross-linked P(NIPAM_{0.75}-*co*-FPMAM_{0.25}) swelled from 1.54 times its dry thickness at 0 V to 1.79 times at 0.5 V and 20 °C, a 16% thickness increase upon oxidation compared to 12% for PFPAM at 20 °C. At 40 °C, P(NIPAM_{0.75}-*co*-FPMAM_{0.25}) swelled from 1.31 times its dry thickness at 0 V to 1.56 at 0.5 V, a 19% increase, which matched 19% for PFPAM at 40 °C. Additionally, P(NIPAM_{0.75}-*co*-FPMAM_{0.25}) showed greater temperature response, with its thickness decreasing 15% when the temperature was increased from 20 to 40 °C at 0 V and 13% at 0.5 V, while the thickness of PFPAM decreased 9.3 and 4.6% for the same temperature change at 0 and 0.5 V, respectively. Cross-linked P(NIPAM_{0.90}-*co*-FPMAM_{0.10}) swelled dramatically from 2.06 times its dry thickness at 0 V to 2.94 times at 0.5 V vs Ag/AgCl, a 43% increase, which was much greater than 16 and 12% for P(NIPAM_{0.75}-*co*-FPMAM_{0.25}) and PFPAM, respectively. Despite having fewer redox units per unit volume, P(NIPAM_{0.9}-*co*-FPMAM_{0.1}) swelled significantly more than P(NIPAM_{0.75}-*co*-FPMAM_{0.25}), and P(NIPAM_{0.75}-*co*-FPMAM_{0.25}) swelled more than PFPAM at 20 °C, indicative of a synergistic effect of NIPAM to incorporate water into the copolymer film upon FPMAM oxidation. That is, the hydration of NIPAM and FPMAM units cannot be treated independently. NIPAM copolymers are known to display composition-dependent LCSTs, where hydrophobic comonomers lower the LCST and hydrophilic comonomers raise the LCST.⁴⁹ The oxidation of FPMAM greatly increases its hydrophilicity, possibly allowing for the NIPAM moieties in P(NIPAM_{0.90}-*co*-FPMAM_{0.10}) to hydrate in an LCST-like transition. Cloud point measurements of lower FPMAM mole fraction (P(NIPAM_{0.95}-*co*-FPMAM_{0.05}) and P(NIPAM_{0.975}-*co*-FPMAM_{0.025})) demonstrated a redox-induced phase transition, where at a fixed temperature above the reduced LCST, oxidation induced complete miscibility of the copolymer (Supporting Information Figure S1-12). These cloud point measurements highlight how the hydrophilicity switch of a small percentage of moieties can change the microenvironment for the entire polymer. The amplified electrochemical morphological response of the P(NIPAM_{0.90}-*co*-FPMAM_{0.10}) film at 20 °C is analogous to oxidation-induced miscibility, where the hydrophilicity switch of a small percentage of moieties triggers an LCST-like phase transition. At 40 °C, this electrochemical response was dampened as P(NIPAM_{0.90}-*co*-FPMAM_{0.10}) swelled from 1.41 times its dry thickness at 0 V to 1.59 times at 0.5 V, a 13% increase compared to 19% for both P(NIPAM_{0.75}-*co*-FPMAM_{0.25}) and PFPAM. The drastic reduction in thickness and electrochemical swelling of P(NIPAM_{0.9}-*co*-FPMAM_{0.1}) with increasing temperature can be explained by the thermoresponsive behavior of NIPAM chains collapsing and expelling water as the temperature increases.

This reduced swelling capability was not due to loss of polymer during the electrochemical cycling, as P(NIPAM_{0.90}-*co*-FPMAM_{0.10}) was quite stable during electrochemical cycling. P(NIPAM_{0.90}-*co*-FPMAM_{0.10}) consistently returned to the same reduced thickness after each subsequent electrochemical cycle (Supporting Information Figure S2-4). Over the 5 electrochemical cycles (1 cycle at each temperature) P(NIPAM_{0.90}-*co*-FPMAM_{0.10}) retained 89% of its charge

(Supporting Information Figure S2-5). When the % thickness increase (also the strain, $\Delta L/L$) is normalized by the charge passed, it was clear that the diminished morphological response of P(NIPAM_{0.90-co}-FPMAM_{0.10}) with increasing temperature is not due to loss of polymer (Figure 2). In fact,

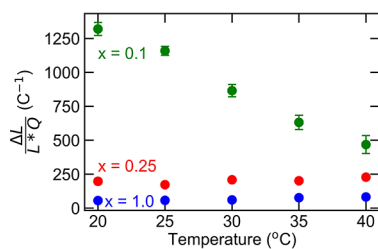


Figure 2. P(NIPAM_{1-x-co}-FPMAM_x) strain/charge ratios. Strain ($\Delta L/L$) is the difference between the oxidized and reduced thickness divided by the reduced thickness.

the greater than 20-fold increase of the strain/charge ratio of P(NIPAM_{0.90-co}-FPMAM_{0.10}) (1320% C⁻¹) as compared to PFPAM (55.6% C⁻¹) suggests that copolymers that encourage solvent swelling could assist electroactive polymer actuator design, especially for applications where a large strain/charge is needed.⁵⁰ Copolymers with higher NIPAM mole fractions (such as P(NIPAM_{0.95-co}-FPMAM_{0.05}) or even higher fractions) did not show significant electrochemical response, perhaps due to the lack of sufficient electroactive units for clear redox-response (Supporting Information Figure S2-7). Charge transport requires electron hopping on ferrocene units, which may be hindered with small fractions of ferrocene.⁵¹

2.2. Reversible Morphological Response by Orthogonal Stimuli

P(NIPAM_{0.90-co}-FPMAM_{0.10}) represents a unique dual thermo-electrochemical-responsive copolymer, which can be swelled significantly through electrochemical input, then deswelled with an increase in temperature back to, or below, its original thickness (Figure 3a). A pure ferrocene polymer

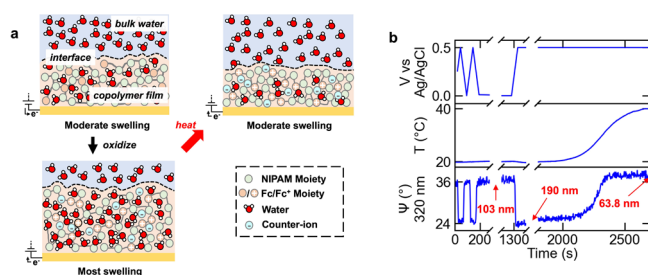


Figure 3. (a) Schematic of P(NIPAM_{0.9-co}-FPMAM_{0.1}) reversible swelling and deswelling through orthogonal stimuli. (b) Dynamic ellipsometric tracking of $\Psi(320\text{ nm})$ through electrochemical swelling then temperature induced deswelling.

(PFPAM) could not achieve this behavior by itself, and this copolymer design approach opens the doors for the independent or synergistic control and actuation of the redox-polymer film by thermal and electrochemical responses. To illustrate this capability, we have modulated the swelling of our copolymer by electric field, and reversibly deswelled by thermal control. Figure 3b shows the dynamic ellipsometric tracking of $\Psi(320\text{ nm})$ for P(NIPAM_{0.90-co}-FPMAM_{0.10}) through the orthogonal input process. During electrochemical

swelling at 20 °C, $\Psi(320\text{ nm})$ reversibly changed from 36° when P(NIPAM_{0.90-co}-FPMAM_{0.10}) is reduced to 24° when P(NIPAM_{0.90-co}-FPMAM_{0.10}) is oxidized. Then, $\Psi(320\text{ nm})$ returns to 38° when the temperature is increased to 40 °C while keeping P(NIPAM_{0.90-co}-FPMAM_{0.10}) oxidized. Ellipsometric spectra were taken where the breaks are shown and this sample of P(NIPAM_{0.90-co}-FPMAM_{0.10}) started at 2.42 times dry thicknesses at 20 °C and 0 V vs Ag/AgCl, swelled 83% to 4.44 times dry thicknesses when the potential was changed to 0.5 V vs Ag/AgCl, then deswelled to 1.49 times dry thicknesses when the temperature was raised to 40 °C (Supporting Information Figure S2-8). These findings serve to illustrate the controllability of the responses for modulating these films, which in the future can lead to multiresponsive systems, in which both thermal or electrochemical responses can be leveraged depending on the availability of thermal or electric gradients.

2.3. Amplified Hydration through Copolymer Design and Electrochemical Control

Electrochemical quartz crystal microbalance (EQCM) was used to gravimetrically track water ingress into P(NIPAM_{1-x-co}-FPMAM_x) films during the oxidation process (Figure 4a). P(NIPAM_{1-x-co}-FPMAM_x) was spin coated and cross-linked on gold-coated EQCM sensors with the same procedure as for ellipsometry. A potential step from 0.0 to 0.5 V vs Ag/AgCl was used to oxidize the copolymer films in 20 mM NaClO₄ and the subsequent current and QCM frequency were monitored (Figure 4b). Figure 4c,d shows examples of the change in electrode mass as a function of the charge passed through the electrode immediately after the oxidative potential switch for PFPAM and P(NIPAM-co-FPMAM) at 30 °C. The measured data are plotted in blue and contain three distinct regions: an initial region of charge accumulation without mass change, a middle region of charge accumulation accompanied by mass gain (plotted in green), and a final region of charge accumulation without mass gain. The quotient of the total change in mass and the total change in faradaic charge, represented by the slope of the black dashed line. The other two regions were ignored because they most likely represent capacitive electric double-layer charging outside the polymer film, which the QCM sensor does not detect. The red dashed line represents the expected mass change if all the faradaic charge passed can be accounted for by the ingress of bare perchlorate ions. The experimentally observed effective slope (black dashed line) is greater than the theoretical slope for bare perchlorate ions and this difference can be accounted for by additional solvent (water) molecules ingressing into the polymer film. Attributing additional mass above which can be accounted for by bare counterions to solvent has been used for polymer films and porous carbon films.^{52,53} Based on the analysis of the EQCM data, 3.83, 13.7, and 565 water molecules entered the polymer films per perchlorate ion when PFPAM, P(NIPAM_{0.75-co}-FPMAM_{0.25}), and P(NIPAM_{0.90-co}-FPMAM_{0.10}) were oxidized at 20 °C, respectively (Figure 4e). In total, PFPAM, P(NIPAM_{0.75-co}-FPMAM_{0.25}), and P(NIPAM_{0.90-co}-FPMAM_{0.10}) ingressed 11.0, 11.9, and 269 mmol cm⁻³ of water (normalized by volume of dry polymer, Supporting Information Table S3-2) at 20 °C and this greatly increased ingress of water with increasing NIPAM mole fraction is consistent with our ellipsometry morphological measurements. Increasing the temperature from 20 to 30 °C to

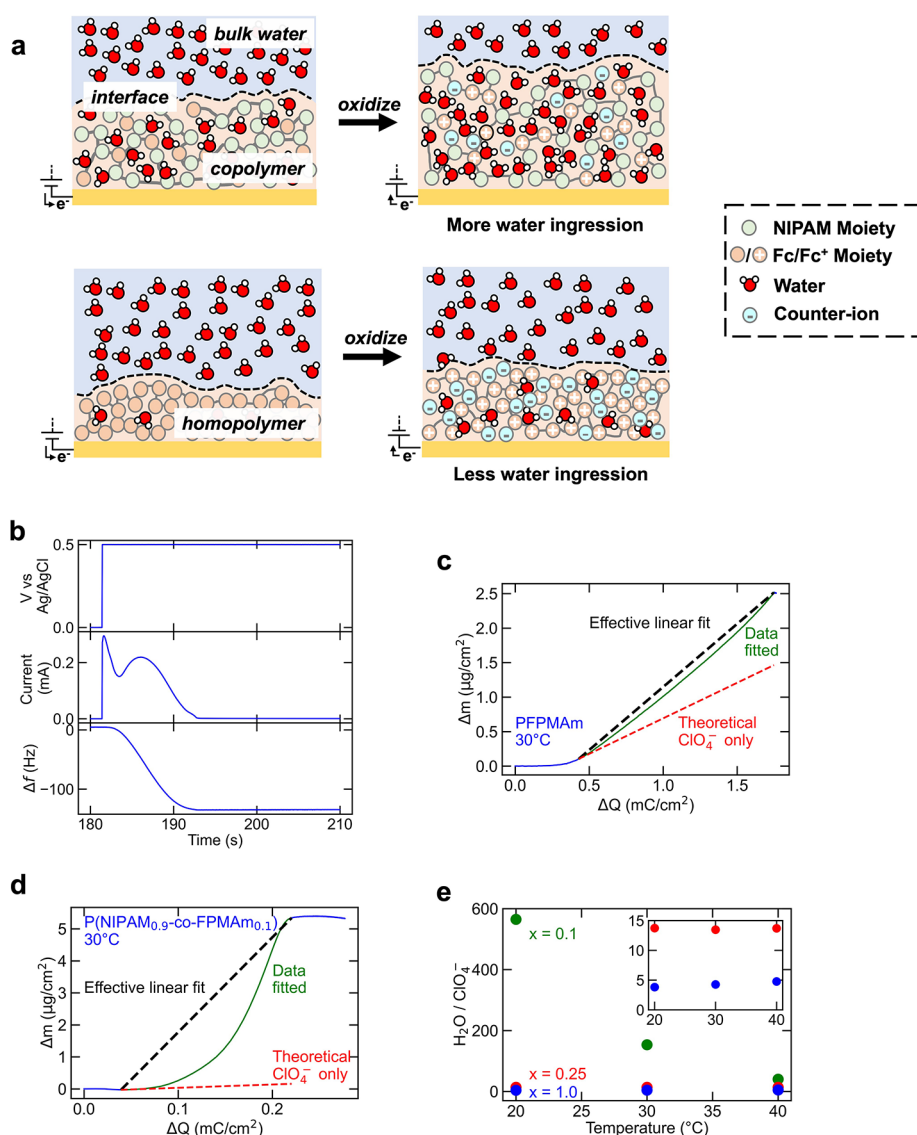


Figure 4. (a) Schematic of water and ion ingress into P(NIPAM_{1-x}-co-FPMAM_x) upon oxidation, through polymer composition, water ingression can be controlled. (b) EQCM current and frequency response of PFPMAm to a potential step from 0 to 0.5 V vs Ag/AgCl at 30 °C in 20 mM NaClO₄. (c) Mass accumulation versus charge passed through the electrode, as calculated from data in (b) for PFPMAm at 30 °C. The red dotted line represents the theoretical mass change of bare perchlorate ions. The black dotted line shows the effective slope of measured mass change vs charge accumulated. The data plotted in green was used for fitting the black dotted line. (d) Same as (c) but for P(NIPAM_{0.9}-co-FPMAM_{0.1}) at 30 °C. (e) Compiled water per perchlorate ion for P(NIPAM_{1-x}-co-FPMAM_x) of various FPMAM at various temperature. Inset: Magnification on $x = 0.25$ and $x = 0.1$.

40 °C, PFPMAm ingressed more water molecules per perchlorate ion from 3.83 to 4.28 to 4.77, respectively (Figure 4e) and ingressed a total of 11.0, 12.4, and 14.0 mmol cm⁻³ water (Supporting Information Tables S3-2). These findings provide qualitative agreement with electrochemical swelling of 0.16, 0.17, and 0.22 dry thicknesses at the same respective temperatures (Figure 1c). The increased ingress of water for PFPMAm with increasing temperature contrasts with the NIPAM containing copolymers, which swelled less electrochemically and ingressed less water as the temperature increased. P(NIPAM_{0.75}-co-FPMAM_{0.25}) ingressed 13.7, 13.5, and 13.7 water molecules per perchlorate at 20, 30, and 40 °C, respectively, and swelled 0.25, 0.24, and 0.25 dry thicknesses at 20, 30, and 40 °C, respectively. P(NIPAM_{0.90}-co-FPMAM_{0.10}) showed the greatest change with temperature. P(NIPAM_{0.90}-co-FPMAM_{0.10}) ingressed 565, 153, and 40.3 water molecules

per perchlorate and a total of 369, 65.2, 18.0 mmol cm⁻³ water at 20, 30, and 40 °C, respectively. In conjunction, the film was electrochemically swelled by 43, 16, and 12%. Clearly, as the temperature increases, NIPAM loses its hydrophilic character and its ability to synergistically bring in water.

2.4. Morphological Insight of P(NIPAM_{0.90}-co-FPMAM_{0.10}) through In Situ NR

P(NIPAM_{0.90}-co-FPMAM_{0.10}) was examined using NR to provide insight into the nanoscale spatial morphology of P(NIPAM_{0.90}-co-FPMAM_{0.10}). NR measurements were performed using the liquids Reflectometer (LR, BL-4B) at the Spallation Neutron Source (SNS) of Oak Ridge National Laboratory (ORNL).⁵⁴ NR provides a powerful tool to investigate complex multilayer thin films under in-situ conditions. The LR is ideal for measuring the surface and interfacial structures of thin films in a horizontal sample

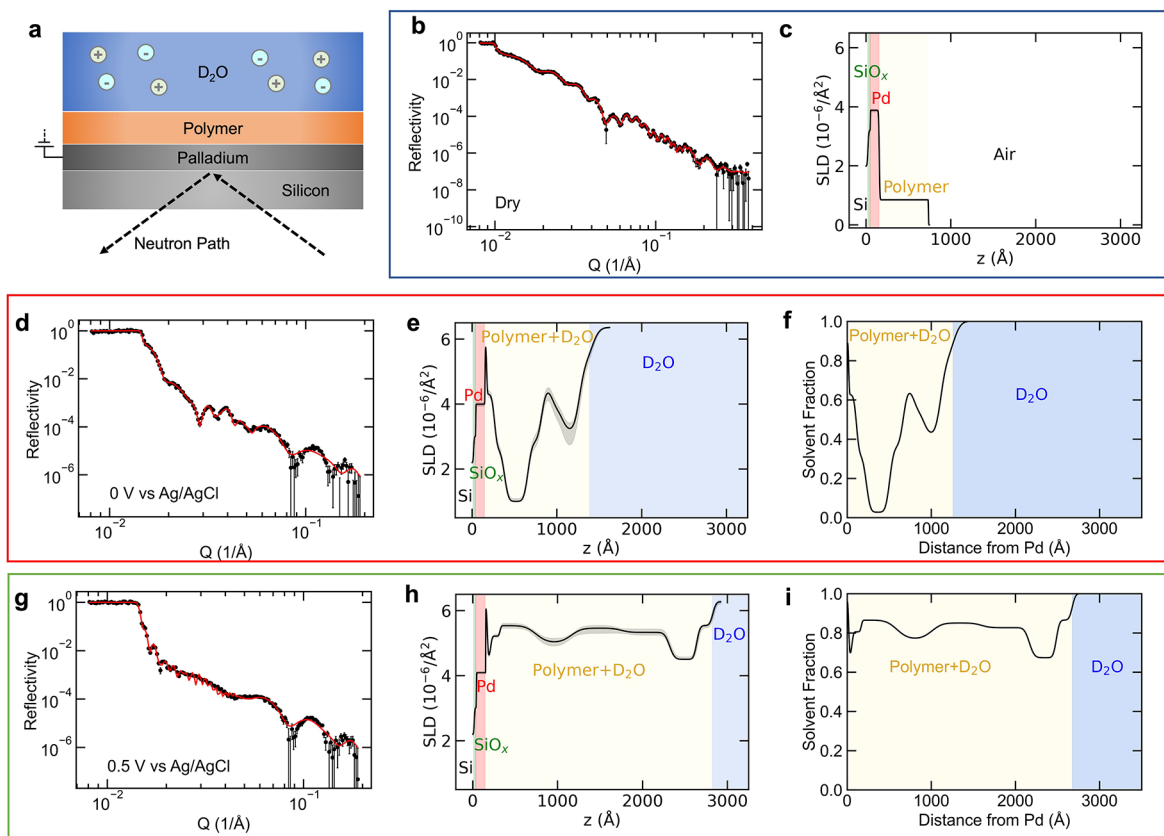


Figure 5. (a) Schematic of NR experiment. Reflectivity profiles for the P(NIPAM_{0.9}-*co*-FPMAM_{0.1}) sample in (b) air, (d) in 20 mM NaClO₄, D₂O at 0 V vs Ag/AgCl, (g) in 20 mM NaClO₄, D₂O at 0.5 V vs Ag/AgCl. Black points represent experimental data, and the red lines represent the best fits. Fitted scattering length density profiles in (c) air, (e) at 0 V vs Ag/AgCl, and (h) at 0.5 V vs Ag/AgCl. The black represents the best fit, and the gray shading adjacent to the best fit represents the 90% confidence interval. Solvent fraction of P(NIPAM_{0.9}-*co*-FPMAM_{0.1}) at (f) 0 V vs Ag/AgCl and (i) 0.5 V vs Ag/AgCl.

geometry, and tracking change of layer thickness, roughness, and scattering length density (SLD) as a function of depth. The SLD of a material is the number density of a particular molecule of atomic species within the scattering volume. The sample used consisted of a Si wafer with 5 mm thickness and 51 mm diameter, which was sputter coated with 10 nm of palladium, then spin coated with P(NIPAM_{0.90}-*co*-FPMAM_{0.10}), and thermally cross-linked, following the same procedure as for samples prepared for ellipsometry. The dry sample was first measured to determine the thickness and SLD of the P(NIPAM_{0.90}-*co*-FPMAM_{0.10}) layer, then examined in 20 mM NaClO₄ with heavy water solvent (D₂O) at 23 °C (Figure 5a). As with ellipsometry, the film was electrochemically cycled prior to the reported measurements to ensure equilibrium conditions are reported rather than the transient behavior of initial swelling. To interpret reflectivity data, a layered model was fitted to the data using software provided by ORNL.^{55,56} The fitted models correspond to the SLD depth profile of the thin film perpendicular to the flat surface of the Si wafer, where the *z* value is 0 Å at the Si wafer surface. The parameters used to generate the fitted model are listed in Supporting Information Table S6. Figure 5b shows the reflectivity profile of dry P(NIPAM_{0.90}-*co*-FPMAM_{0.10}) in air, and Figure 5c shows the best fit SLD profile having a polymer layer that is 580 Å thick and has an SLD of 0.85. After contact with the NaClO₄ solution and electrochemical cycling, the reflectivity was measured at 0 V vs Ag/AgCl (Figure 5d) and Figure 5e shows the fitted SLD profile. The sample in solution was

modeled with the palladium layer parameters obtained from the dry state measurement, on which we added nine layers to form a freeform SLD distribution within the overall thickness constraint set by our ellipsometry measurements. A Markov Chain Monte Carlo optimizer (DREAM) was used to sample the posterior distribution of solutions, which can be used to calculate the uncertainty of each parameter.⁵⁷ To assess the stability of our fits, the distribution of solutions obtained from the Markov chain was used to compute a two-sided 90% confidence level interval for the SLD value at each *z* value. The thickness of P(NIPAM_{0.90}-*co*-FPMAM_{0.10}) increased significantly to 1260 Å, qualitatively consistent with previous ellipsometric measurements, and the SLD of the polymer layer has increased due to the ingress of D₂O. However, the polymer SLD profile is no longer uniform but has several peaks and valleys. To assign a physical interpretation to the SLD profile, a solvent fraction profile was determined using the following equation:

$$\varphi(\text{D}_2\text{O}) = \frac{\text{SLD}_{\text{film}} - \text{SLD}_0}{\text{SLD}_{\text{D}_2\text{O}} - \text{SLD}_0}$$

Figure 5f shows the solvent fraction profile for P(NIPAM_{0.90}-*co*-FPMAM_{0.10}) at 0 V. At the polymer–palladium interface, there is a small region of high solvation. This layer of solvation has been shown before between polyvinylferrocene films on gold surfaces.⁴⁶ We hypothesize that this charged metal surface is more hydrophilic than the polymer, thus

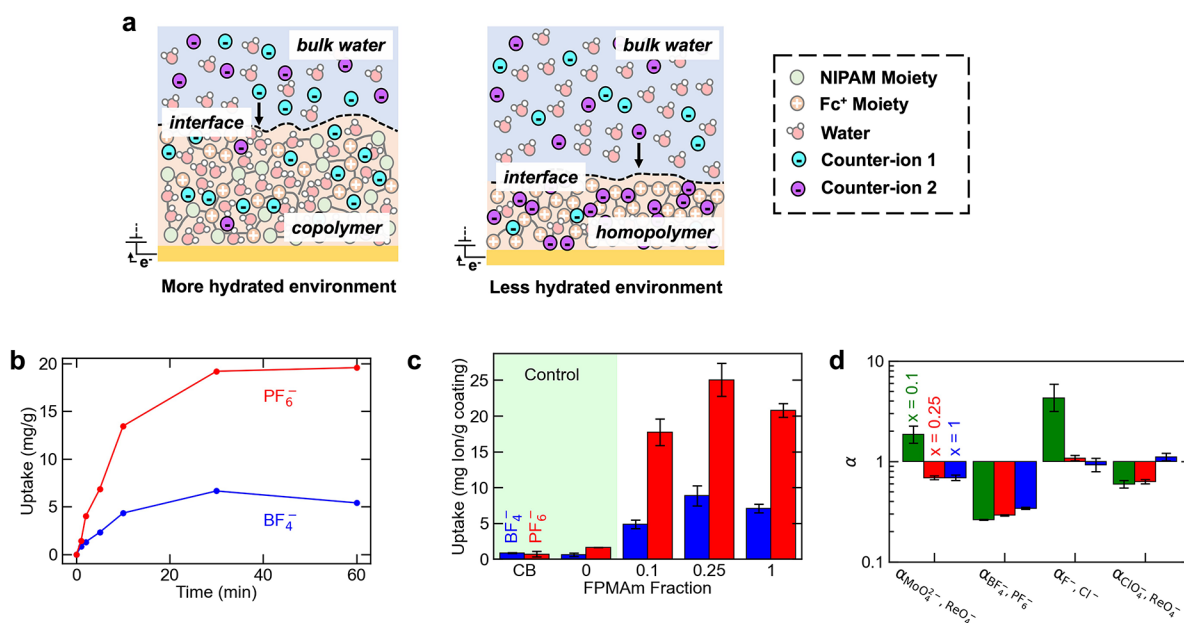


Figure 6. (a) Schematic of how changing copolymer ratio can be changed to control hydration and ion selectivity. (b) Adsorption kinetics of P(NIPAM_{0.9}-co-FPMAM_{0.1})-CB at a 2 V applied cell voltage. (c) Removal of BF₄⁻, PF₆⁻, from 0.5 mM NaBF₄ and 0.5 mM NaPF₆ using P(NIPAM_{1-x}-co-FPMAM_x)-CB electrodes with a 2 V cell potential. Data represented by mean ± standard deviation for *N* = 2 replicates. (d) Compiled separation factors of P(NIPAM_{1-x}-co-FPMAM_x)-CB with various FPMAM fraction. Data represented by geometric mean and range for *N* = 2 replicates.

solvent can stay trapped at this surface when expelled from the polymer. Within the bulk of the polymer film, there is a significant dip in solvent fraction to 0.03 around 400 Å away from the palladium surface, where we hypothesize a phase-separated region of hydrophobic ferrocene moieties aggregated together. Beyond this layer of polymer phase-separated region, there is one smaller valley at ~1000 Å and solvent fraction ~0.4, then a gradual gradient of increasing solvation until the solvent front. Upon oxidation to 0.5 V vs Ag/AgCl, small fringes appear in the reflectivity profile in the low *Q* region (Figure 5g), resulting in features of longer length scales in the SLD profile and the polymer film has expanded to 2680 Å (Figure 5h). The solvation profile at 0.5 V vs Ag/AgCl still has the small region of high solvation near the palladium interface, however, the deep valley of phase-separated polymer is no longer present (Figure 5i). Instead, the solvation profile is much flatter and more solvated up to ~0.8 solvent fraction. This flattening of the SLD and solvation profiles is hypothesized to be an LCST-type transition. The transformation of hydrophobic ferrocene moieties into hydrophilic ferrocenium moieties dramatically increases solvation, allowing these moieties to mix better with the rest of the polymer. This behavior in turn allows for the adjacent NIPAM moieties to hydrate in an LCST-like transition, resulting in a significantly higher solvation profile with much smaller variations in solvent fraction, modulated solely by electrochemical potential.

It should be noted that this treatment of solvent fraction ignores the ingress of perchlorate anions, which have a positive SLD.⁴⁶ However, the fraction of perchlorate is ignored as being too small to significantly affect the SLD. At 20 mM, NaClO₄ represents 0.04 mol percent of solution species, so the SLD changes at 0 V vs Ag/AgCl are 99.96% from D₂O. Additional perchlorate ingresses at 0.5 V vs Ag/AgCl; however, it was determined that perchlorate represents a small mole fraction (1/566 or 0.17%) of the total species ingressed so the

SLD changes at 0.5 V vs Ag/AgCl can be assumed to be mostly due to D₂O.

2.5. Tunable Ion Interactions through Hydrophilicity/Hydrophobicity

From ellipsometry and EQCM, it was determined that the control of the NIPAM to FPMAM ratio allows for rational control of hydrophilicity and the tuning of the water content within the copolymers based on chemical structure. As a consequence, the tunable hydration of P(NIPAM_{1-x}-co-FPMAM_x) provides a viable platform for studying the effect of polymer solvation on ion selectivity, with the potential for leveraging these effects for selective electroadsorption (Figure 6a).

This approach allows for a dedicated investigation of solvation effects, independent of structural changes to the ferrocenium site, and thus without directly changing the charge-transfer properties of the redox center itself. Electrodes of carbon black (CB), P(NIPAM_{1-x}-co-FPMAM_x), and benzene-1,3-disulfonyl azide were made using a solution processing method (Methods section) to form P(NIPAM_{1-x}-co-FPMAM_x)-CB electrodes (Supporting Information Figure S4-8). Selectivity was probed using binary electroadsorption tests with P(NIPAM_{1-x}-co-FPMAM_x)-CB electrodes in 0.5 mM of two different anions as sodium salts. A 2 V bias was applied across the P(NIPAM_{1-x}-co-FPMAM_x)-CB working electrode and a counter platinum electrode. Figure 6b shows a typical electroadsorption kinetic profile for P(NIPAM_{0.9}-co-FPMAM_{0.1})-CB from 0.5 mM NaBF₄ + 0.5 mM NaPF₆, and Figure 6c compiles the adsorption uptakes of P(NIPAM_{1-x}-co-FPMAM_x)-CB with various FPMAM fractions and for CB without polymer from 0.5 mM NaBF₄ + 0.5 mM NaPF₆ after 30 min. PNIPAM-CB and CB alone showed little to no removal of any anion with CB adsorbing 0.87 mg g⁻¹ BF₄⁻ and 0.71 mg g⁻¹ PF₆⁻ and PNIPAM-CB adsorbing 0.62 mg g⁻¹ BF₄⁻ and 1.6 mg g⁻¹ PF₆⁻. The addition of FPMAM greatly

increased the adsorption of anions with P(NIPAM_{0.9-co}-FPMAM_{0.1})-CB adsorbing 4.9 mg g⁻¹ BF₄⁻ and 17.7 mg g⁻¹ PF₆⁻, P(NIPAM_{0.75-co}-FPMAM_{0.25})-CB adsorbing 8.9 mg g⁻¹ BF₄⁻ and 25.0 mg g⁻¹ PF₆⁻, and PFPAM-CB adsorbing 7.07 mg g⁻¹ BF₄⁻ and 20.8 mg g⁻¹ PF₆⁻. The separation factor, $\alpha_{A,B}$, was used to quantify selectivity between two anions, A and B:

$$\alpha_{A,B} = \frac{N_{A,ads}/N_{B,ads}}{N_{A,sol}/N_{B,sol}}$$

where $N_{A,ads}$ and $N_{B,ads}$ are the moles of A and B adsorbed on the electrode, respectively, and $N_{A,sol}$ and $N_{B,sol}$ are the moles of A and B remaining in the solution, respectively.

The selectivity of P(NIPAM_{1-x-co}-FPMAM_x)-CB toward various anions changed depending on the copolymer fraction. $\alpha_{BF_4^-, PF_6^-}$ increased slightly from 0.26 to 0.29 to 0.34, as the FPMAM fraction changed from 0.1 to 0.25 to 1, respectively (Figure 6d). Similar experiments were performed with ClO₄⁻ + ReO₄⁻, Cl⁻ + F⁻, and MoO₄²⁻ + ReO₄⁻ ion pairs. $\alpha_{ClO_4^-, ReO_4^-}$ increased from 0.59 to 0.63 to 1.1, α_{F^-, Cl^-} decreased from 4.3 to 1.1 to 0.92, and $\alpha_{MoO_4^{2-}, ReO_4^-}$ decreased from 1.8 to 0.697 to 0.696 as FPMAM fraction changed from 0.1 to 0.25 to 1, respectively (Figure 6d). The trend in selectivity between F⁻ and Cl⁻ (α_{F^-, Cl^-}) is perhaps the easiest to explain. F⁻ is a smaller ion, hence has a higher charge density, and is a stronger solvated ion than Cl⁻.⁵⁸ Making the surface more hydrophilic with a higher NIPAM fraction shifts the selectivity in favor of the higher solvated ion. The change in selectivity with copolymer composition is not due to the uptake of ions from the NIPAM component, as PNIPAM-CB did not significantly uptake any ions. The selectivity between MoO₄²⁻ and ReO₄⁻, $\alpha_{MoO_4^{2-}, ReO_4^-}$, followed the same trend as for α_{F^-, Cl^-} , as increasing NIPAM fraction increased the selectivity for MoO₄²⁻, the stronger solvated ion (Supporting Information Table S5-1). Divalent ions, such as MoO₄²⁻, are typically solvated much more strongly than monovalent ions.⁵⁸

In the case of ClO₄⁻ and ReO₄⁻, reducing the FPMAM fraction shifts the selectivity in favor of ReO₄⁻, despite ReO₄⁻ being the larger and less hydrated ion. This trend may be due to the stronger interaction of ReO₄⁻ with water than ClO₄⁻, as would be predicted by their conjugate acid pK_a's.⁵⁹⁻⁶¹ If ReO₄⁻ interacts less with water, as would be predicted by pK_a, then this experimental selectivity trend is consistent with the selectivity trend between F⁻ and Cl⁻ if water-induced ion pairing is the primary mechanism for ion binding. Another explanation may rely on localized charges within the ion, as Re is less electronegative than Cl, a more negative charge may be located on the oxygens in ReO₄⁻ than in ClO₄⁻, and the solvent may preferentially interact with this localized charge.¹¹ However, some previously reported Hofmeister series have suggested ReO₄⁻ has weaker interactions with water than ClO₄⁻.⁶² Similarly, P(NIPAM_{1-x-co}-FPMAM_x)-CB films showed consistently higher selectivity for PF₆⁻ over BF₄⁻, regardless of FPMAM fraction, and this selectivity increased slightly when the FPMAM fraction was decreased. This trend more closely resembles the selectivity trend between ReO₄⁻ and ClO₄⁻, where selectivity for the larger ion increased as the FPMAM fraction decreased. While correlations for many physicochemical phenomena can be interpreted based on these ion trends (size, hydration, Hofmeister), it should be noted specific ion effects are still not fully understood and there are plentiful examples of the breaking and rearrangement of these

ion series.^{11,63} Thus, a deeper mechanistic understanding of some cases requires detailed future studies, especially to fully elucidate and predict the ion-selectivity trends that may fall outside the expected ion series, or have less sensitivity to the effects.

Clearly, changing the FPMAM fraction in P(NIPAM_{1-x-co}-FPMAM_x)-CB changes the ion selectivity. The highest selectivity shift observed in this study occurred for α_{F^-, Cl^-} , which decreased from 4.3 to 0.92 (a factor of 4.6) as the FPMAM fraction changed from 0.1 to 1. This magnitude of selectivity shift is comparable to the previous report investigating the effects of polymer structure on ion selectivity (a factor of 7.6 between polyvinylferrocene and polyferrocenylsilane for the VO₃⁻ + CrO₄⁻ ion).¹⁸ The selectivity shift between polyvinylferrocene and polyferrocenylsilane was attributed to the pendant versus main-chain structural difference and charge-transfer modulation of a silane group. While the ions tested are different, the similar shifts in selectivity may suggest that the solvation effects leveraged by switching from P(NIPAM_{0.9-co}-FPMAM_{0.1}) to FPMAM can be as potent as steric and charge-transfer effects when determining ion selectivity. Finally, some ion pairs tested were either extremely selective toward one ion such that a selectivity factor could not be accurately determined (e.g., close to full selectivity), or the ions were electrochemically reactive themselves (Supporting Information Figure S4-(4-7)). While further studies and a broader scope of ion pairs are needed to elucidate all the specific ion effects that determine selectivity and yield the resulting separation factors, we have demonstrated that the P(NIPAM_{1-x-co}-FPMAM_x) platform can decouple the effects of surface hydrophilicity/hydrophobicity and charge-transfer to elucidate deeper mechanistic understanding of specific ion interactions with redox electroactive surfaces. In the long term, our work provides a new strategy for overcoming the limitations in the design of single-site redox units. By taking advantage of macromolecular control, we can tune polymer solvation environment based on multifunctional stimulus and, consequently, achieve desired ion selectivity beyond charge-transfer effects.

3. CONCLUSIONS

Incorporation of NIPAM, a thermoresponsive moiety, with FPMAM, a redox-responsive moiety, yielded P(NIPAM_{1-x-co}-FPMAM_x) films which displayed temperature and electric potential dependent morphology, as probed by in-situ ellipsometry and neutron reflectometry. The findings from the current work provide fundamental insights into materials design for multiresponsive redox materials, with multidimensional control over morphology changes, solvation, ion ingress, and selectivity between ions. P(NIPAM_{0.9-co}-FPMAM_{0.1}) showed the greatest electrochemical response, swelling from 2.06 times its dry thickness at 0 V to 2.94 times at 0.5 V vs Ag/AgCl at 20 °C, and the greatest thermoresponse, deswelling from 2.94 to 1.59 times the dry thicknesses as the temperature was increased to 40 °C. The increased electrochemical morphological response of P(NIPAM_{0.9-co}-FPMAM_{0.1}) and P(NIPAM_{0.75-co}-FPMAM_{0.25}) over PFPAM suggests that NIPAM synergistically enhances water ingress within the polymer film upon oxidation, in which the transformation of FPMAM from a hydrophobic to hydrophilic species increases the hydrophilicity of the NIPAM environment and induces a local LCST-like transition. This synergistic solvation effect was quantified with EQCM, with

P(NIPAM_{0.9-co}-FPMAm_{0.1}) enabling the ingress of 565 water molecules per perchlorate ion, a difference of more than 2 orders of magnitude as compared to PFPMAm, which ingressed 3.83 water molecules per perchlorate at 20 °C. In total, P(NIPAM_{0.9-co}-FPMAm_{0.1}) ingressed 269 mmol cm⁻³ water, as compared to 11.0 mmol cm⁻³ for PFPMAm. The water per perchlorate ratio and total water ingress decreased greatly for P(NIPAM_{0.9-co}-FPMAm_{0.1}) as the temperature increased and only 40.3 water molecules per perchlorate were ingressed at 40 °C, accounting for a total of 18.0 mmol cm⁻³ water. In contrast, the water per perchlorate ratio increased for PFPMAm from 3.83 at 20 °C to 4.77 at 40 °C, and total water ingress increased from 11.0 to 14.0 mmol cm⁻³. NR data provided nanoscale solvent distribution information, and it was observed that P(NIPAM_{0.9-co}-FPMAm_{0.1}), at 0 V vs Ag/AgCl, was 1260 Å thick and had a layer of highly phase-separated polymer at only 0.03 solvent fraction before a gradual solvation front of smooth SLD change to pure D₂O. Upon oxidation to 0.5 V vs Ag/AgCl, the P(NIPAM_{0.9-co}-FPMAm_{0.1}) film expanded to 2680 Å and the hydrophobic phase separated regions smoothed out with the rest of the polymer film to around 0.8 solvent fraction. Our work provides, for the first time, unique insights into the spatially resolved in situ solvation of redox-copolymers under electrochemical potential. P(NIPAM_{1-x-co}-FPMAm_x)-CB electrodes were used to investigate how surface hydrophilicity affects ion selectivity. PFPMAm-CB and P(NIPAM_{0.9-co}-FPMAm_{0.1}) showed almost a fivefold difference in selectivity as α_{F^-, Cl^-} decreased from 4.3 to 0.92, respectively. Here, we have mainly leveraged these copolymers to decouple polymer hydration from charge-transfer effects, to access new modes for controlling ion selectivity.

Beyond electrochemical separations, there is untapped potential in using P(NIPAM_{1-x-co}-FPMAm_x) as a dual-responsive material for various applications. In particular, the amplified morphological response of P(NIPAM_{1-x-co}-FPMAm_x) by electrochemistry, as compared to PFPMAm, suggests that copolymer design can promote solvent ingress and possibly even enhance electroactive polymer actuator response. At the same time, the deswelling of P(NIPAM_{1-x-co}-FPMAm_x) with an increase in temperature may allow its application as a dual-responsive actuator or polyelectrolyte with a built-in thermal safety mechanism.^{50,64} The amplified thermo- and electrochemically responsive hydration of P(NIPAM_{1-x-co}-FPMAm_x) may allow for the electrification of drug delivery systems, which typically utilize thermoresponsive changes in hydration for real-time tuning of drug release, or even for smart surfaces with dual-responsive wettability.^{22,65} For ferrocene and other electro-responsive polymers, the selectivity results obtained with different copolymer ratios of P(NIPAM_{1-x-co}-FPMAm_x) represent how the degree of hydration of the local environment surrounding the ferrocene binding sites can play a significant role in determining ion interactions. Thus, future design of electro-responsive polymers for targeted ion separations can focus not only on the modulation of polymer–ion interactions but also leverage polymer–solvent interactions to enhance desired selectivity behavior.

4. EXPERIMENTAL SECTION/METHODS

4.1. Copolymer Synthesis

Ferrocenylpropyl methacrylamide (FPMAm) was synthesized as described elsewhere.⁶⁶ *N*-isopropylacrylamide (NIPAM) (TCI Chemicals) was recrystallized in hexane before use. NIPAM and FPMAm (14 mmol total) were dissolved in 6 mL of 1,4-dioxane with 0.14 mmol 2,2'-azobis(2-methylpropionitrile) (Sigma). The solution was purged with argon for 20 min and then heated to 60 °C for 16 h while stirring. After polymerization, the solution was diluted with THF and precipitated in cold diethyl ether, twice. The product was left to dry under vacuum overnight. Extended synthesis yields and polymer characterization are available in the [Supporting Information](#).

4.2. In Situ Electrochemical Ellipsometry

P(NIPAM_{1-x-co}-FPMAm_x) and an additional 10 wt % benzene-1,3-disulfonyl azide were dissolved in chloroform (5 mg/mL), filtered with 0.2 μm nylon, and spin-coated (2000 rpm, 1 min, 1000 rpm/s acceleration) on gold-coated sapphire glass slides. The spin-coated samples were heated in a 160 °C oven for 1 h to induce the cross-linking reaction. An ellipsometry electrochemical cell with an angle of incidence of 70° (redox.me) was mounted on a J.A. Woollam VASE ellipsometer, and 20 mM NaClO₄ was pumped between the cell and a heated water bath. The temperature was monitored at the outlet of a cell with a platinum resistance temperature detector (Pt-RTD) (100 ohms at 0 °C) plus an amplifier with the resistance read by an Arduino. Spectroscopic ellipsometric measurements were made between 300 and 1000 nm and copolymer films were modeled as Cauchy materials using J.A. Woollam WVASE software. Examples of modeling fits are provided in the [Supporting Information](#). Electrochemical measurements were made using a Squidstat Solo potentiostat (Admiral Instruments), Ag/AgCl reference electrode, and Pt wire counter electrode. Before ellipsometric measurement, copolymer films were cycled with CVs until the peak current no longer increased with each cycle. Starting at the lowest temperature for each set of measurements, ellipsometric measurement was taken at a reducing potential before scanning to the oxidizing potential at 10 mV/s. The potential was returned to the reducing potential before the temperature was increased.

4.3. EQCM

EQCM was performed using a BluQCM QSD unit (Biologic) with a QSD-TCU to control the temperature. Electrochemical and temperature measurements were made in the provided AWS Mirage software with an SP-200 potentiostat (Biologic). Copolymer films were spin coated on 5 MHz Cr/Au 14 mm wrapped QCM sensors (Quartz Pro) and heated in a 160 °C oven for 1 h. Prior to the presented mass per charge data, copolymer films were cycled in 20 mM NaClO₄ until peak current no longer increased. Starting at the lowest temperature, mass per charge data were obtained using a potential step from 0 V vs Ag/AgCl to 0.5 V vs Ag/AgCl. Once the mass no longer increased, the potential was returned to 0 V and the temperature was increased. The QCM frequency was interpreted following rigid or viscoelastic criteria.^{67,68} Films that met the rigid criteria were modeled using the Sauerbrey equation and films that did not meet the rigid criteria were fitted to a Voigt viscoelastic model.^{69–71} Further details of frequency interpretation and examples of mass per charge data are provided in the [Supporting Information](#).

4.4. Neutron Reflectometry

NR experiments were carried out on the LR at the SNS at ORNL in Oak Ridge, TN, United States. A complete reflectivity measurement is made of seven instrument configurations taken at different incident angles (θ) between 0.6° and 2.343° and neutron wavelengths (λ) between 2.5 and 18.5 Å. The measured intensity of the reflected neutron beam is usually expressed in terms of the wavevector transfer Q and is defined by the incident angle θ and neutron wavelength λ :

$$Q = \frac{4\pi \sin \theta}{\lambda}$$

Data were fit using the REFL1D software package, accessed through the ORNL-provided web interface.^{55,56} The fitted models correspond to the SLD depth profile $\beta(z)$ of the thin film perpendicular to the flat surface of the Si wafer, where the z value is 0 Å at the Si wafer surface.

4.5. Binary Ion Separations

To create P(NIPAM_{1-x}-co-FPMAM_x)-CB electrodes, 20 mg of copolymer and 2 mg of benzene-1,3-disulfonyl azide were dissolved in 4 mL of chloroform then 20 mg of CB, acetylene (Alfa Aesar) was added and sonicated in icy water. This solution was added in 50 μ L drops onto Toray Carbon Paper 030 5% wet proofed (Fuel Cell Store) and oven-dried between drops until 4 drops were added. After coating, the electrodes were left in a 160 °C oven for 1 h. For binary ion separation tests, the P(NIPAM_{1-x}-co-FPMAM_x)-CB were submerged in 1.5 mL of solution containing 0.5 mM of two sodium salts (NaCl and NaF, NaBF₄ and NaPF₆, or NaClO₄ and NaReO₄) with a platinum wire counter electrode, then charged at 2 V vs the counter electrode for 30 min. The electrodes were removed from the solution while the electrochemical potential (of 2 V) was still applied. The solution was assayed for ion concentration [IC (Thermo Scientific Dionex Inegron—AS22 column) for Cl⁻, F⁻, ClO₄⁻, and ICP-OES (Agilent 5110) for BF₄⁻, PF₆⁻, ReO₄⁻]. Uptake was calculated using the following formula:

$$\text{Uptake} = \frac{C_0 - C}{m_{\text{electrode coating}}} V$$

where C_0 was the initial mass basis concentration of an ion, C was the concentration of the ion after adsorption, $m_{\text{electrode coating}}$ was the mass of P(NIPAM_{1-x}-co-FPMAM_x)-CB on the electrode, and V was the volume of the solution. To quantify a separation factor, the following equation was used:

$$\alpha_{A,B} = \frac{N_{A,\text{ads}}/N_{B,\text{ads}}}{N_{A,\text{sol}}/N_{B,\text{sol}}}$$

where $N_{A,\text{ads}}$ and $N_{B,\text{ads}}$ are the moles of A and B adsorbed on the electrode, respectively, and $N_{A,\text{sol}}$ and $N_{B,\text{sol}}$ are the moles of A and B remaining in the solution, respectively.

■ ASSOCIATED CONTENT

SI Supporting Information

The Supporting Information is available free of charge at <https://pubs.acs.org/doi/10.1021/jacsau.3c00486>.

Additional experimental details, materials, methods, and characterization data, including EQCM data, polymer characterization, and neutron reflectivity fits (PDF)

■ AUTHOR INFORMATION

Corresponding Author

Xiao Su – Department of Chemical and Biomolecular Engineering, University of Illinois Urbana–Champaign, Urbana, Illinois 61801, United States; orcid.org/0000-0001-7794-290X; Email: x2su@illinois.edu

Authors

Raylin Chen – Department of Chemical and Biomolecular Engineering, University of Illinois Urbana–Champaign, Urbana, Illinois 61801, United States

Hanyu Wang – Neutron Scattering Division and Center for Nanophase Materials Sciences, Oak Ridge National Laboratory, Oak Ridge, Tennessee 37831, United States

Mathieu Doucet – Neutron Scattering Division, Oak Ridge National Laboratory, Oak Ridge, Tennessee 37831, United States; orcid.org/0000-0002-5560-6478

James F. Browning – Neutron Scattering Division, Oak Ridge National Laboratory, Oak Ridge, Tennessee 37831, United States

Complete contact information is available at: <https://pubs.acs.org/doi/10.1021/jacsau.3c00486>

Author Contributions

CRediT: Raylin Chen conceptualization, data curation, formal analysis, investigation, methodology, validation, visualization, writing-original draft, writing-review & editing; Hanyu Wang data curation, formal analysis, investigation, methodology, resources, writing-review & editing; Mathieu Doucet data curation, formal analysis, methodology, software, writing-review & editing; James F. Browning data curation, formal analysis, investigation, methodology, resources, visualization, writing-review & editing; Xiao Su conceptualization, formal analysis, funding acquisition, investigation, project administration, writing-original draft, writing-review & editing.

Funding

US Department of Energy, Basic Energy Sciences Award DE-SC0021409.

Notes

The authors declare no competing financial interest.

■ ACKNOWLEDGMENTS

This work was supported by the US Department of Energy, Basic Energy Sciences Award DE-SC0021409. Ellipsometry and XPS were carried out in the Materials Research Laboratory Central Research Facilities, University of Illinois. A portion of this research used resources at the SNS, a Department of Energy (DOE) Office of Science User Facility operated by ORNL. Neutron reflectometry measurements were carried out on the Liquids Reflectometer at the SNS, which is sponsored by the Scientific User Facilities Division, Office of Basic Energy Sciences, DOE. ORNL is managed by UT-Battelle LLC for the DOE under Contract DE-AC05-00OR22725. The authors thank Johannes Elbert for providing the FPMAM monomer, helping with interpreting NMR spectra, and performing copolymerization kinetic experiments. The authors thank Ching-Yu Chen for help with LCST measurements.

■ REFERENCES

- (1) Yan, D.; Wang, Z.; Zhang, Z. Stimuli-Responsive Crystalline Smart Materials: From Rational Design and Fabrication to Applications. *Acc. Chem. Res.* **2022**, *55* (7), 1047–1058.
- (2) Schattling, P.; Jochum, F. D.; Theato, P. Multi-stimuli responsive polymers – the all-in-one talents. *Polym. Chem.* **2014**, *5* (1), 25–36.
- (3) Ouimet, J. A.; Xu, J.; Flores - Hansen, C.; Phillip, W. A.; Boudouris, B. W. Design Considerations for Next-Generation Polymer Sorbents: From Polymer Chemistry to Device Configurations. *Macromol. Chem. Phys.* **2022**, *223* (16), No. 2200032.
- (4) Dahlman, C. J.; LeBlanc, G.; Bergerud, A.; Staller, C.; Adair, J.; Milliron, D. J. Electrochemically Induced Transformations of Vanadium Dioxide Nanocrystals. *Nano Lett.* **2016**, *16* (10), 6021–6027.
- (5) Srimuk, P.; Su, X.; Yoon, J.; Aurbach, D.; Presser, V. Charge-transfer materials for electrochemical water desalination, ion separation and the recovery of elements. *Nat. Rev. Mater.* **2020**, *5* (7), 517–538.
- (6) Cotty, S.; Jeon, J.; Elbert, J.; Jeyaraj, V. S.; Mironenko, A. V.; Su, X. Electrochemical recycling of homogeneous catalysts. *Sci. Adv.* **2022**, *8* (42), No. eade3094.

- (7) Su, X.; Kushima, A.; Halliday, C.; Zhou, J.; Li, J.; Hatton, T. A. Electrochemically-mediated selective capture of heavy metal chromium and arsenic oxyanions from water. *Nat. Commun.* **2018**, *9* (1), 4701.
- (8) Su, X. Electrochemical interfaces for chemical and biomolecular separations. *Curr. Opin. Colloid Interface Sci.* **2020**, *46*, 77–93.
- (9) Cheung, M. S.; García, A. E.; Onuchic, J. N. Protein folding mediated by solvation: Water expulsion and formation of the hydrophobic core occur after the structural collapse. *Proc. Natl. Acad. Sci. U. S. A.* **2002**, *99* (2), 685–690.
- (10) Blokzijl, W.; Engberts, J. B. F. N. Hydrophobic Effects. Opinions and Facts. *Angew. Chem., Int. Ed. Engl.* **1993**, *32* (11), 1545–1579.
- (11) Gregory, K. P.; Elliott, G. R.; Robertson, H.; Kumar, A.; Wanless, E. J.; Webber, G. B.; Craig, V. S. J.; Andersson, G. G.; Page, A. J. Understanding specific ion effects and the Hofmeister series. *Phys. Chem. Chem. Phys.* **2022**, *24* (21), 12682–12718.
- (12) Ma, C. D.; Wang, C.; Acevedo-Vélez, C.; Gellman, S. H.; Abbott, N. L. Modulation of hydrophobic interactions by proximally immobilized ions. *Nature* **2015**, *517* (7534), 347–350.
- (13) Chen, X.; Qian, P.; Zhang, T.; Xu, Z.; Fang, C.; Xu, X.; Chen, W.; Wu, P.; Shen, Y.; Li, S.; Wu, J.; Zheng, B.; Zhang, W.; Huo, F. Catalyst surfaces with tunable hydrophilicity and hydrophobicity: metal–organic frameworks toward controllable catalytic selectivity. *Chem. Commun.* **2018**, *54* (32), 3936–3939.
- (14) Mao, X.; Tian, W.; Ren, Y.; Chen, D.; Curtis, S. E.; Buss, M. T.; Rutledge, G. C.; Hatton, T. A. Energetically efficient electrochemically tunable affinity separation using multicomponent polymeric nanostructures for water treatment. *Energy Environ. Sci.* **2018**, *11* (10), 2954–2963.
- (15) Schwierz, N.; Horinek, D.; Netz, R. R. Reversed Anionic Hofmeister Series: The Interplay of Surface Charge and Surface Polarity. *Langmuir* **2010**, *26* (10), 7370–7379.
- (16) Schwierz, N.; Horinek, D.; Sivan, U.; Netz, R. R. Reversed Hofmeister series—The rule rather than the exception. *Curr. Opin. Colloid Interface Sci.* **2016**, *23*, 10–18.
- (17) Su, X.; Kulik, H. J.; Jamison, T. F.; Hatton, T. A. Anion-Selective Redox Electrodes: Electrochemically Mediated Separation with Heterogeneous Organometallic Interfaces. *Adv. Funct. Mater.* **2016**, *26* (20), 3394–3404.
- (18) Chen, R.; Feng, J.; Jeon, J.; Sheehan, T.; Rüttiger, C.; Gallei, M.; Shukla, D.; Su, X. Structure and Potential-Dependent Selectivity in Redox-Metallopolymers: Electrochemically Mediated Multicomponent Metal Separations. *Adv. Funct. Mater.* **2021**, *31* (15), No. 2009307.
- (19) Halperin, A.; Kröger, M.; Winnik, F. M. Poly(N-isopropylacrylamide) Phase Diagrams: Fifty Years of Research. *Angew. Chem., Int. Ed.* **2015**, *54* (51), 15342–15367.
- (20) Futscher, M. H.; Philipp, M.; Müller-Buschbaum, P.; Schulte, A. The Role of Backbone Hydration of Poly(N-isopropyl acrylamide) Across the Volume Phase Transition Compared to its Monomer. *Sci. Rep.* **2017**, *7* (1), 17012.
- (21) Bischofberger, I.; Calzolari, D. C. E.; De Los Rios, P.; Jelezarov, I.; Trappe, V. Hydrophobic hydration of poly-N-isopropyl acrylamide: a matter of the mean energetic state of water. *Sci. Rep.* **2014**, *4* (1), 4377.
- (22) Alarcón, C. D. L. H.; Pennadam, S.; Alexander, C. Stimuli responsive polymers for biomedical applications. *Chem. Soc. Rev.* **2005**, *34* (3), 276–285.
- (23) Tang, L.; Wang, L.; Yang, X.; Feng, Y.; Li, Y.; Feng, W. Poly(N-isopropylacrylamide)-based smart hydrogels: Design, properties and applications. *Prog. Mater. Sci.* **2021**, *115*, No. 100702.
- (24) Xu, X.; Bizmark, N.; Christie, K. S. S.; Datta, S. S.; Ren, Z. J.; Priestley, R. D. Thermoresponsive Polymers for Water Treatment and Collection. *Macromolecules* **2022**, *55* (6), 1894–1909.
- (25) *Ferrocenes*, Štěpnička, P., Ed. Wiley, 2008.
- (26) Patra, M.; Gasser, G. The medicinal chemistry of ferrocene and its derivatives. *Nat. Rev. Chem.* **2017**, *1* (9), No. 0066.
- (27) Pietschnig, R. Polymers with pendant ferrocenes. *Chem. Soc. Rev.* **2016**, *45* (19), 5216–5231.
- (28) Hailes, R. L. N.; Oliver, A. M.; Gwyther, J.; Whittell, G. R.; Manners, I. Polyferrocenylsilanes: synthesis, properties, and applications. *Chem. Soc. Rev.* **2016**, *45* (19), 5358–5407.
- (29) Elbert, J.; Gallei, M.; Rüttiger, C.; Brunsen, A.; Didzoleit, H.; Stühn, B.; Rehahn, M. Ferrocene Polymers for Switchable Surface Wettability. *Organometallics* **2013**, *32* (20), 5873–5878.
- (30) Akhoury, A.; Bromberg, L.; Hatton, T. A. Redox-Responsive Gels with Tunable Hydrophobicity for Controlled Solubilization and Release of Organics. *ACS Appl. Mater. Interfaces* **2011**, *3* (4), 1167–1174.
- (31) Su, X.; Hatton, T. A. Redox-electrodes for selective electrochemical separations. *Adv. Colloid Interface Sci.* **2017**, *244*, 6–20.
- (32) Su, X.; Tan, K.-J.; Elbert, J.; Rüttiger, C.; Gallei, M.; Jamison, T. F.; Hatton, T. A. Asymmetric Faradaic systems for selective electrochemical separations. *Energy Environ. Sci.* **2017**, *10* (5), 1272–1283.
- (33) Kim, K.; Cotty, S.; Elbert, J.; Chen, R.; Hou, C.-H.; Su, X. Asymmetric Redox-Polymer Interfaces for Electrochemical Reactive Separations: Synergistic Capture and Conversion of Arsenic. *Adv. Mater.* **2020**, *32* (6), No. 1906877.
- (34) Liu, X.; Zhao, L.; Liu, F.; Astruc, D.; Gu, H. Supramolecular redox-responsive ferrocene hydrogels and microgels. *Coord. Chem. Rev.* **2020**, *419*, No. 213406.
- (35) Irie, M.; Tanaka, T. *Polym. Prepr., Jpn.* **1991**, *40*, 461.
- (36) Kuramoto, N.; Shishido, Y. Property of thermo-sensitive and redox-active poly(N-cyclopropylacrylamide-co-vinylferrocene) and poly(N-isopropylacrylamide-co-vinylferrocene). *Polymer* **1998**, *39* (3), 669–673.
- (37) Oyama, N.; Tatsuma, T.; Takahashi, K. Electrochemical characterization of a thermoresponsive N-isopropylacrylamide-vinylferrocene copolymer film by the use of quartz crystal oscillators. *J. Phys. Chem.* **1993**, *97* (40), 10504–10508.
- (38) Tatsuma, T.; Takada, K.; Matsui, H.; Oyama, N. A Redox Gel. Electrochemically Controllable Phase Transition and Thermally Controllable Electrochemistry. *Macromolecules* **1994**, *27* (22), 6687–6689.
- (39) Kaniewska, K.; Romański, J.; Karbarz, M. Oxidation of ferrocenemethanol grafted to a hydrogel network through cysteine for triggering volume phase transition. *RSC Adv.* **2013**, *3* (45), 23816–23823.
- (40) Marcisz, K.; Mackiewicz, M.; Romanski, J.; Stojek, Z.; Karbarz, M. Significant, reversible change in microgel size using electrochemically induced volume phase transition. *Appl. Mater. Today* **2018**, *13*, 182–189.
- (41) Du, P.; Liu, J.; Chen, G.; Jiang, M. Dual Responsive Supramolecular Hydrogel with Electrochemical Activity. *Langmuir* **2011**, *27* (15), 9602–9608.
- (42) Zhang, Q. M.; Berg, D.; Duan, J.; Mugo, S. M.; Serpe, M. J. Optical Devices Constructed from Ferrocene-Modified Microgels for H₂O₂ Sensing. *ACS Appl. Mater. Interfaces* **2016**, *8* (40), 27264–27269.
- (43) Sui, X.; Feng, X.; Di Luca, A.; van Blitterswijk, C. A.; Moroni, L.; Hempenius, M. A.; Vancso, G. J. Poly(N-isopropylacrylamide)-poly(ferrocenylsilane) dual-responsive hydrogels: synthesis, characterization and antimicrobial applications. *Polym. Chem.* **2013**, *4* (2), 337–342.
- (44) Feng, X.; Zhang, K.; Chen, P.; Sui, X.; Hempenius, M. A.; Liedberg, B.; Vancso, G. J. Highly Swellable, Dual-Responsive Hydrogels Based on PNIPAM and Redox Active Poly(ferrocenylsilane) Poly(ionic liquid)s: Synthesis, Structure, and Properties. *Macromol. Rapid Commun.* **2016**, *37* (23), 1939–1944.
- (45) Mergel, O.; Schneider, S.; Tiwari, R.; Kühn, P. T.; Keskin, D.; Stuart, M. C. A.; Schöttner, S.; de Kanter, M.; Noyong, M.; Caumanns, T.; Mayer, J.; Janzen, C.; Simon, U.; Gallei, M.; Wöll, D.; van Rijn, P.; Plamper, F. A. Cargo shuttling by electrochemical switching of core–shell microgels obtained by a facile one-shot polymerization. *Chem. Sci.* **2019**, *10* (6), 1844–1856.

- (46) Glidle, A.; Hillman, A. R.; Ryder, K. S.; Smith, E. L.; Cooper, J.; Gadegaard, N.; Webster, J. R. P.; Dalgliesh, R.; Cubitt, R. Use of Neutron Reflectivity to Measure the Dynamics of Solvation and Structural Changes in Polyvinylferrocene Films During Electrochemically Controlled Redox Cycling. *Langmuir* **2009**, *25* (7), 4093–4103.
- (47) Gettler, R.; Young, M. J. Multimodal cell with simultaneous electrochemical quartz crystal microbalance and in operando spectroscopic ellipsometry to understand thin film electrochemistry. *Rev. Sci. Instrum.* **2021**, *92* (5), No. 053902.
- (48) Schuh, K.; Prucker, O.; Rühle, J. Surface Attached Polymer Networks through Thermally Induced Cross-Linking of Sulfonyl Azide Group Containing Polymers. *Macromolecules* **2008**, *41* (23), 9284–9289.
- (49) Jain, K.; Vedarajan, R.; Watanabe, M.; Ishikiriyama, M.; Matsumi, N. Tunable LCST behavior of poly(N-isopropylacrylamide/ionic liquid) copolymers. *Polym. Chem.* **2015**, *6* (38), 6819–6825.
- (50) Madden, P. G. A.; Madden, J. D. W.; Anquetil, P. A.; Vandesteeg, N. A.; Hunter, I. W. The relation of conducting polymer actuator material properties to performance. *IEEE J. Oceanic Eng.* **2004**, *29* (3), 696–705.
- (51) Akhoury, A.; Bromberg, L.; Hatton, T. A. Interplay of Electron Hopping and Bounded Diffusion during Charge Transport in Redox Polymer Electrodes. *J. Phys. Chem. B* **2013**, *117* (1), 333–342.
- (52) Tsai, W.-Y.; Taberna, P.-L.; Simon, P. Electrochemical Quartz Crystal Microbalance (EQCM) Study of Ion Dynamics in Nanoporous Carbons. *J. Am. Chem. Soc.* **2014**, *136* (24), 8722–8728.
- (53) Wang, S.; Li, F.; Easley, A. D.; Lutkenhaus, J. L. Real-time insight into the doping mechanism of redox-active organic radical polymers. *Nat. Mater.* **2019**, *18* (1), 69–75.
- (54) Ankner, J. F.; Tao, X.; Halbert, C. E.; Browning, J. F.; Michael Kilbey, S.; Swader, O. A.; Dadmun, M. S.; Kharlampieva, E.; Sukhishvili, S. A. The SNS Liquids Reflectometer. *Neutron News* **2008**, *19* (3), 14–16.
- (55) Doucet, M.; Ferraz Leal, R. M.; Hobson, T. C. Web interface for reflectivity fitting. *SoftwareX* **2018**, *7*, 287–293.
- (56) Kienzle, P. A.; O'Donovan, K. V.; Ankner, J. F.; Berk, N. F.; Majkrzak, C. F. *REFLID*; 2017
- (57) Vrugt, J. A.; ter Braak, C. J. F.; Diks, C. G. H.; Robinson, B. A.; Hyman, J. M.; Higdon, D. Accelerating Markov Chain Monte Carlo Simulation by Differential Evolution with Self-Adaptive Randomized Subspace Sampling. *Int. J. Nonlinear Sci. Numer. Simul.* **2009**, *10* (3), 273–290, DOI: 10.1515/IJNSNS.2009.10.3.273.
- (58) Marcus, Y. Thermodynamics of solvation of ions. Part 5—Gibbs free energy of hydration at 298.15 K. *J. Chem. Soc., Faraday Trans.* **1991**, *87* (18), 2995–2999.
- (59) McDonald, F. E.; Towne, T. B.; Schultz, C. C. Metal-oxo induced syn-oxidative polycyclizations of hydroxypolyenes: Biomimetic synthesis of polycyclic ether natural products. *Pure Appl. Chem.* **1998**, *70* (2), 355–358, DOI: 10.1351/pac199870020355.
- (60) Trummal, A.; Lipping, L.; Kaljurand, I.; Koppel, I. A.; Leito, I. Acidity of Strong Acids in Water and Dimethyl Sulfoxide. *J. Phys. Chem. A* **2016**, *120* (20), 3663–3669.
- (61) Chu, B.; Whitney, D. C.; Diamond, R. M. On anion-exchange resin selectivities. *J. Inorg. Nucl. Chem.* **1962**, *24* (11), 1405–1415.
- (62) Jordan, J. H.; Gibb, C. L. D.; Wishard, A.; Pham, T.; Gibb, B. C. Ion–Hydrocarbon and/or Ion–Ion Interactions: Direct and Reverse Hofmeister Effects in a Synthetic Host. *J. Am. Chem. Soc.* **2018**, *140* (11), 4092–4099.
- (63) Kang, B.; Tang, H.; Zhao, Z.; Song, S. Hofmeister Series: Insights of Ion Specificity from Amphiphilic Assembly and Interface Property. *ACS Omega* **2020**, *5* (12), 6229–6239.
- (64) Kelly, J. C.; Pepin, M.; Huber, D. L.; Bunker, B. C.; Roberts, M. E. Reversible Control of Electrochemical Properties Using Thermally-Responsive Polymer Electrolytes. *Adv. Mater.* **2012**, *24* (7), 886–889.
- (65) Li, F.; Zhu, Y.; Wang, Y. Dual-responsive drug delivery system with real time tunable release behavior. *Microporous Mesoporous Mater.* **2014**, *200*, 46–51.
- (66) Vapnik, H.; Elbert, J.; Su, X. Redox-copolymers for the recovery of rare earth elements by electrochemically regenerated ion-exchange. *J. Mater. Chem. A* **2021**, *9* (35), 20068–20077.
- (67) Easley, A. D.; Ma, T.; Eneh, C. I.; Yun, J.; Thakur, R. M.; Lutkenhaus, J. L. A practical guide to quartz crystal microbalance with dissipation monitoring of thin polymer films. *J. Polym. Sci.* **2022**, *60* (7), 1090–1107.
- (68) Reviakine, I.; Johannsmann, D.; Richter, R. P. Hearing What You Cannot See and Visualizing What You Hear: Interpreting Quartz Crystal Microbalance Data from Solvated Interfaces. *Anal. Chem.* **2011**, *83* (23), 8838–8848.
- (69) Voinova, M. V.; Rodahl, M.; Jonson, M.; Kasemo, B. Viscoelastic Acoustic Response of Layered Polymer Films at Fluid-Solid Interfaces: Continuum Mechanics Approach. *Phys. Scr.* **1999**, *59* (5), 391–396.
- (70) McNamara, T. P.; Blanford, C. F. A sensitivity metric and software to guide the analysis of soft films measured by a quartz crystal microbalance. *Analyst* **2016**, *141* (10), 2911–2919.
- (71) Saftics, A.; Prószyński, G. A.; Türk, B.; Peter, B.; Kurunczi, S.; Horvath, R. In situ viscoelastic properties and chain conformations of heavily hydrated carboxymethyl dextran layers: a comparative study using OWLS and QCM-I chips coated with waveguide material. *Sci. Rep.* **2018**, *8* (1), 11840.